Clinical Kidney Journal, 2023, vol. 16, no. 12, 2639–2651

https://doi.org/10.1093/ckj/sfad215
Advance Access Publication Date: 25 October 2023
Original Article

ORIGINAL ARTICLE

Molecular characteristics of circulating B cells and kidney cells at the single-cell level in special types of primary membranous nephropathy

Xiaoqian Feng[1], Qilin Chen[1], Jinjie Zhong[1], Sijie Yu[1], Yue Wang[2], Yaru Jiang[1], Junli Wan[1], Longfei Li[2], Huimin Jiang[1], Liping Peng[1], Anshuo Wang[1], Gaofu Zhang[1], Mo Wang[1], Haiping Yang[1] and Qiu Li[1]

[1]Department of Nephrology Children's Hospital of Chongqing Medical University, National Clinical Research Center for Child Health and Disorders, Ministry of Education Key Laboratory of Child Development and Disorders, Chongqing Key Laboratory of Pediatrics, Chongqing, China and [2]Nanjing Jiangbei New Area Biopharmaceutical Public Service Platform, Nanjing, Jiangsu, China

Correspondence to: Haiping Yang and Qiu Li; E-mail: oyhp0708@163.com and liqiu809@hospital.cqmu.edu.cn

ABSTRACT

Background. Although primary membranous nephropathy (pMN) associated with podocyte autoantibodies (POS) is becoming well-known, the molecular characteristics of the specific type of pMN that is negative for podocyte autoantibodies (NEG) is still unclear.

Methods. We performed single-cell transcriptome sequencing and single-cell B cell receptor sequencing on circulating $CD19^+$ cells and kidney cells of a NEG paediatric patient with pMN. The single-cell datasets of POS patients and healthy control individuals were included for integrative analysis.

Results. The gene expression characteristics and clonal expansion of naïve and memory B cells in the NEG patient changed significantly. We found that a group of $CD38^+$ naïve B cells expanded in the NEG patient, which had the functional characteristics of cell activation. In addition, the conversion between immunoglobulin M (IgM)/IgD and IgG1 in the NEG patient was increased. Parietal epithelial cells (PECs) and podocytes shared similar signature genes (*WT1*, *CLIC5*), and new candidate marker genes for PECs, such as *NID2*, *CAV1* and *THY1*, might contribute to the definition of cell subsets. PECs might have undergone significant changes in the disease, mainly manifested by changes in the expression of *CCN2*, *PLAAT4* and *SEPTIN2*. The scores of gene sets related to extracellular matrix, cell adhesion and calcium channel in podocytes of the NEG patient was significantly increased. The gene expression of sodium transporter in a group of proximal tubule cells in the disease was significantly increased, especially *SLC5A12*, which might be related to the oedema of patients.

Conclusions. Our research demonstrated the cell type–specific molecular features in the circulation and kidney of the NEG pMN patient.

Received: 12.5.2023; Editorial decision: 2.8.2023

GRAPHICAL ABSTRACT

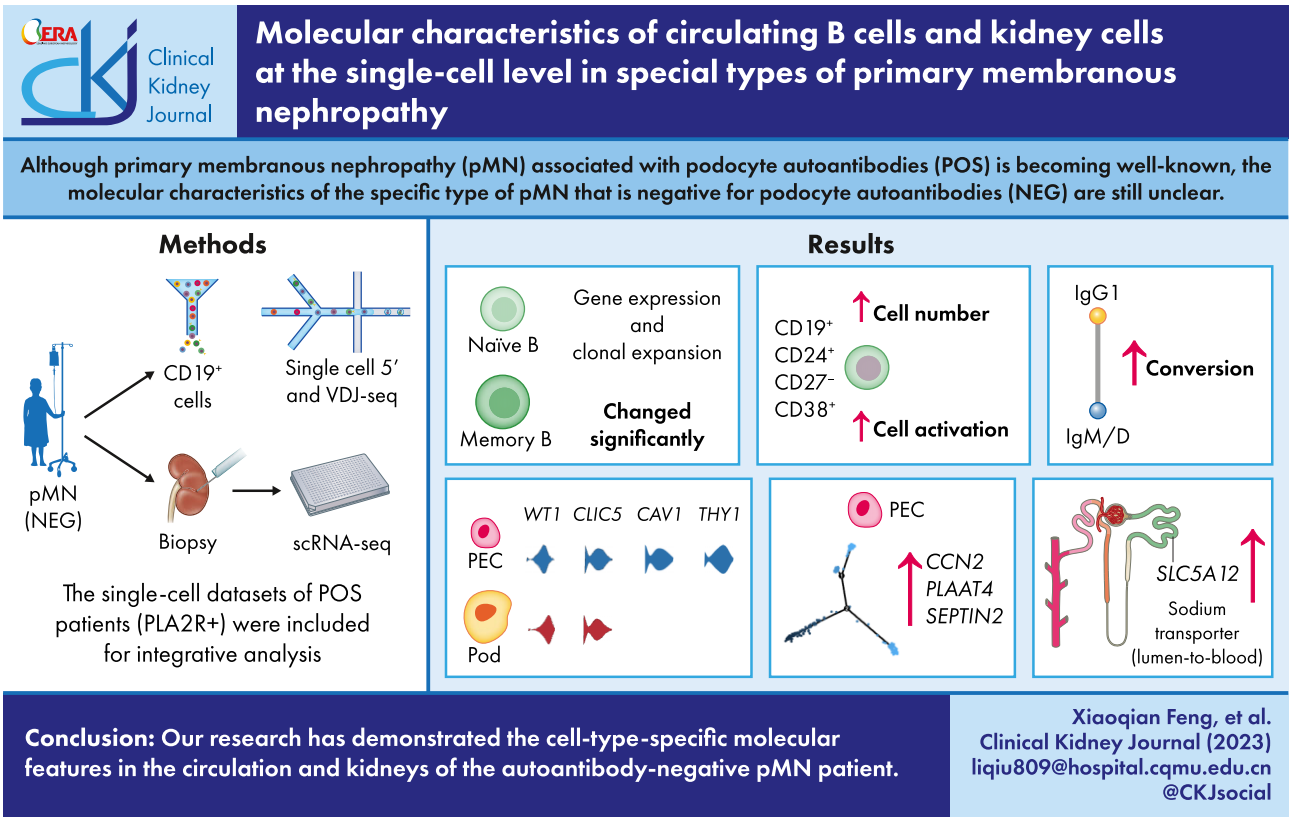

Keywords: B cells, podocytes, primary membranous nephropathy, scBCR-seq, scRNA-seq

INTRODUCTION

Membranous nephropathy (MN) is one of the most common causes of nephrotic syndrome (NS) in adults but is seen less commonly in children [1]. MN is defined as primary MN (pMN) when circulating autoantibodies are present and its target antigen is endogenously expressed on podocytes [2, 3]. Approximately 70% of adult patients with pMN are associated with phospholipase A2 receptor (PLA2R) antigen, and the situation is similar for adolescent patients [4]. In the past decade, new podocyte antigens, including thrombospondin domain-containing 7A (THSD7A) [5], neural EGFL-like 1 (NELL1) [6], semaphorin-3B (SEMA3B) [7] and others [8], have been discovered.

Autoantibodies produced by autoreactive B cells are key drivers of immune pathogenesis in MN [4, 9]. In the acute phase of pMN, the proportion of naïve B cells increases, while the proportion of switched memory B cells and unswitched memory B cells decreases [10]. The frequencies of circulating plasma cells and regulatory B (Breg) cells are significantly higher in MN patients than in both non-immune-mediated chronic kidney disease patients and healthy individuals [11]. A study of B cell receptor (BCR) in MN patients found that among the immunoglobulin heavy-chain variable region (IGHV), the frequency of IGHV3 was lower, while the frequency of IGHV4 was higher [12]. Recent research found that MN has a glomerular transcriptional signature that is enriched in targets of the transcription factor nuclear factor κB, which distinguishes it from other glomerulonephropathies [13]. Accumulating evidence suggests that there are cellular and molecular changes in the circulation and kidney tissue in pMN, but such evidence is mainly from the study of podocyte autoantibody-positive pMN (POS) [14, 15].

At present, it is unclear whether different pathogenic antibodies have different cellular and molecular characteristics because there is a lack of research on non-PLA2R pMN patients and some identified podocyte-associated autoantibody-negative pNMs The investigation of such patients will help to further understand the pathogenesis of pMN. Therefore, we performed single-cell transcriptome sequencing (scRNA-seq) and single-cell BCR sequencing (scBCR-seq) on circulating CD19$^+$ cells and kidney cells of a paediatric patient with pMN who was negative for seven common podocyte autoantibodies (NEG).

MATERIALS AND METHODS

Ethical approval

This study was approved by the Ethics Committee of Children's Hospital Affiliated to Chongqing Medical University (file number: 2022 NO.124). The consent of paediatric patients and their guardians was obtained before sample collection.

Participant details

A paediatric patient with pMN was admitted to the Inpatient Department of Nephrology, Children's Hospital Affiliated with Chongqing Medical University. This patient was negative

for seven autoantibodies and was included in the study (Supplementary Table S1). The validation cohort for flow cytometry analysis included nine paediatric patients with primary NS (Supplementary Table S2).

Processing of peripheral CD19$^+$ cells in scRNA-seq and scBCR-seq

Peripheral blood mononuclear cells (PBMCs) were frozen and thawed according to the 10X Genomics recommended protocol (CG00039). They were incubated with CD19-FITC antibody (11-0199-42; eBioscience, San Diego, CA, USA). CD19$^+$ cells were sorted by flow cytometry (FACSAria III; BD Bioscience, Franklin, Lakes, NJ, USA). The cell viability was >80%. CD19$^+$ single-cell suspensions were diluted to a concentration of 240 cells/μl and loaded onto the Chromium Single Cell Controller (10X Genomics, Pleasanton, CA, USA). Libraries were constructed with a Chromium Single Cell 5′ GEM Library & Gel Bead Kit following the 10X Genomics Chromium protocol (PN-1000263). BCR libraries were constructed with a Chromium Single Cell V(D)J Enrichment Kit (Human B Cell; 10X Genomics). Libraries were sequenced by a NovaSeq 6000 (Illumina, San Diego, CA, USA).

Cell Ranger (version 6.1.2; 10X Genomics) was used to process raw reads for single-cell 5′ gene expression. The human reference data file refdata-gex-GRCh38-2020-A was used. All samples were integrated by Seurat (version 4.1.0). The quality standards are provided in Supplementary Table S3. Gene expression was normalized by the NormalizeData function in the Seurat R package. The first 2000 highly variable genes were chosen by the FindVariableFeatures function for principal component analysis (PCA). The BCR sequences of each B cell were assembled by the Cell Ranger vdj pipeline (version 6.1.2). Chain complementary determining region 3 (CDR3) sequences, rearranged full-length V(D)J fragments and clonotypes were obtained. The human reference data file refdatacellranger-vdj-GRCh38-alts-ensembl-3.1.0 was used.

Processing of kidney scRNA-seq

Residual kidney biopsy tissue after meeting clinical need was stored in GEXSCOPE tissue preservation solution (Singleron Biotechnologies, Köln, Germany) immediately and transported at 4°C [15, 16]. It was then cut up, digested and put into GEXSCOPE tissue dissociation solution (Singleron Biotechnologies 1200050003). The cell viability exceeded 81.4%. The kidney single-cell suspensions were diluted to a concentration of 400 cells/μl and loaded onto the Matrix Single Cell Controller (Singleron Biotechnologies). Libraries were constructed with a GEXSCOPE Single Cell RNA Library Kit (Singleron Biotechnologies). Libraries were sequenced using a HiSeq X10 (Illumina). CeleScope (version 1.8.1) was used to process raw reads for single-cell 3′ gene expression. The human reference data file refdata-cellranger-GRCh38-3.0.0 was used.

Analysis of scRNA-seq of peripheral CD19$^+$ cells and kidney cells

Batch effects between datasets were removed before downstream analysis. The graph-based clustering algorithm was used for clustering and constructs a K-nearest neighbour graph for unsupervised clustering of cells. Cells were visualized in two-dimensional space using uniform manifold approximation and projection (UMAP) algorithms. Highly variable genes of each cluster were identified by the FindAllMarkers function. The FindMarkers function was used for differentially expressed gene (DEG) analysis. An absolute value of $\log_2$ fold-change >0.25 and a *P*-value <.05 were considered significant. Gene ontology (GO) and Kyoto Encyclopedia of Genes and Genomes (KEGG) enrichment analyses were performed by the Metascape webtool (www.metascape.org) and clusterProfiler (version 4.2.2). The R package Monocle2 (version 2.18.0) was used to construct pseudotime trajectories. Gene set-based scores (Supplementary Table S4) were calculated by the AddModuleScore function from Seurat.

BCR analysis

Differences of the VJ pairing between the healthy control group (CTRL) and NEG patient were compared by the DESeq2 (version 1.30.1) package. VJ pairings with an absolute value of $\log_2$ fold-change >1 and a *P*-value <.05 were considered significant. Circos 0.69 was used to display the ring graph. The clone size was defined as the number of times a clonotype was expanded. The clonotypes were mapped to UMAP plots according to the corresponding barcode. Somatic hypermutation (SHM) was assessed using the shazam (version 1.1.0) package. The clonality was clustered using the Change-O (version 1.3.0) package, and the immunoglobulin (Ig) class switch recombination (CSR) was assessed in the same cluster.

Flow cytometry analysis

PBMCs were isolated from 1 ml of venous blood and incubated with the following antibodies: CD19-APC (302212), CD24-BV421 (311121), CD27-FITC (356403) and CD38-PE (303506) (all from BioLegend, San Diego, CA, USA). The expression of B cell surface markers was evaluated by flow cytometry (FASCCanto; BD Biosciences). The datasets were analysed using FlowJo (version 10.8.1; FlowJo, Ashland, OR, USA).

Statistical analysis

Seurat R package (version 4.1.0) and GraphPad Prism software (version 9.4.0; GraphPad Software, San Diego, CA, USA) were used for statistical analysis. Data produced by Seurat R package were analysed using the Wilcoxon rank sum test. Unpaired *t*-tests and one-way analysis of variance were used for comparisons between two and three groups of normally distributed variables, respectively. The Mann–Whitney *U* test and Kruskal–Wallis test were used for comparisons between two and three groups of non-normally distributed variables, respectively. Adjusted *P*-values were calculated by the Benjamini–Hochberg test. A *P*-value <.05 indicated statistical significance.

RESULTS

Significant changes in naïve B cells and memory B cells in the NEG patient

A 10-year-old boy presented with massive proteinuria, hypoalbuminemia and hyperlipidaemia (Supplementary Figure S1A). We diagnosed him with stage III MN according to the pathological manifestations (Supplementary Figure S1B). Immunofluorescence results of seven types of podocyte autoantibodies in the kidney were negative, including PLA2R, THSD7A, SEMA3B, NELL1, exotosin 1 (EXT1), exotosin 2 (EXT2) and protocadherin 7 (PCDH7). The patient was negative for serum anti-PLA2R and THSD7A antibodies (Supplementary Table S1). We named him NEG. At this time, NEG was treated with sufficient

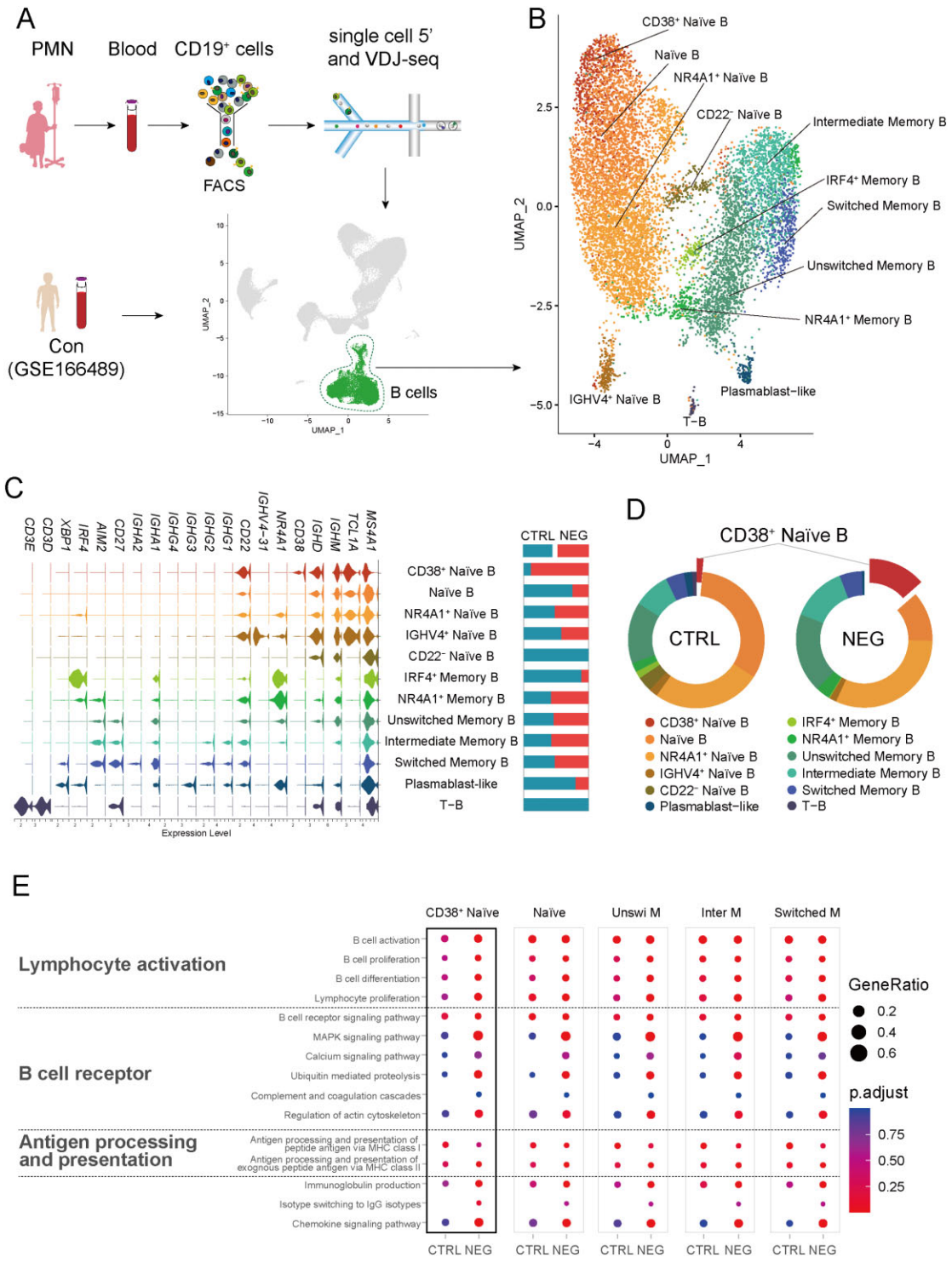

Figure 1: Molecular features of peripheral blood B cells in NEG. **(A)** The experimental workflow of scRNA-seq and scBCR-seq of peripheral blood B cells. **(B)** UMAP plots of B cells from all merged samples, coloured by cell type. Each dot represents an individual cell. **(C)** Violin plots of the selected marker genes in all B cell types. Bar plots show the proportion of CTRL and NEG in each cell type. Blue and red represent samples collected from CTRL and NEG. **(D)** Donut plots show the proportion of each cell type in CTRL and NEG. The proportion of CD38⁺ naïve B cells was increased in NEG compared with CTRL. **(E)** Functional enrichment analysis of CTRL and NEG in each B cell type. GO and KEGG terms shown come from Supplementary Figure S2D. The size of dots represents the proportion of genes enriched to each term and the redder colour key indicates the smaller adjusted *P*-value. CD38⁺ Naïve: CD38⁺ naïve B; Naïve: naïve B; Unswi M: unswitched memory B; Inter M: intermediate memory B; Switched M: switched memory B.

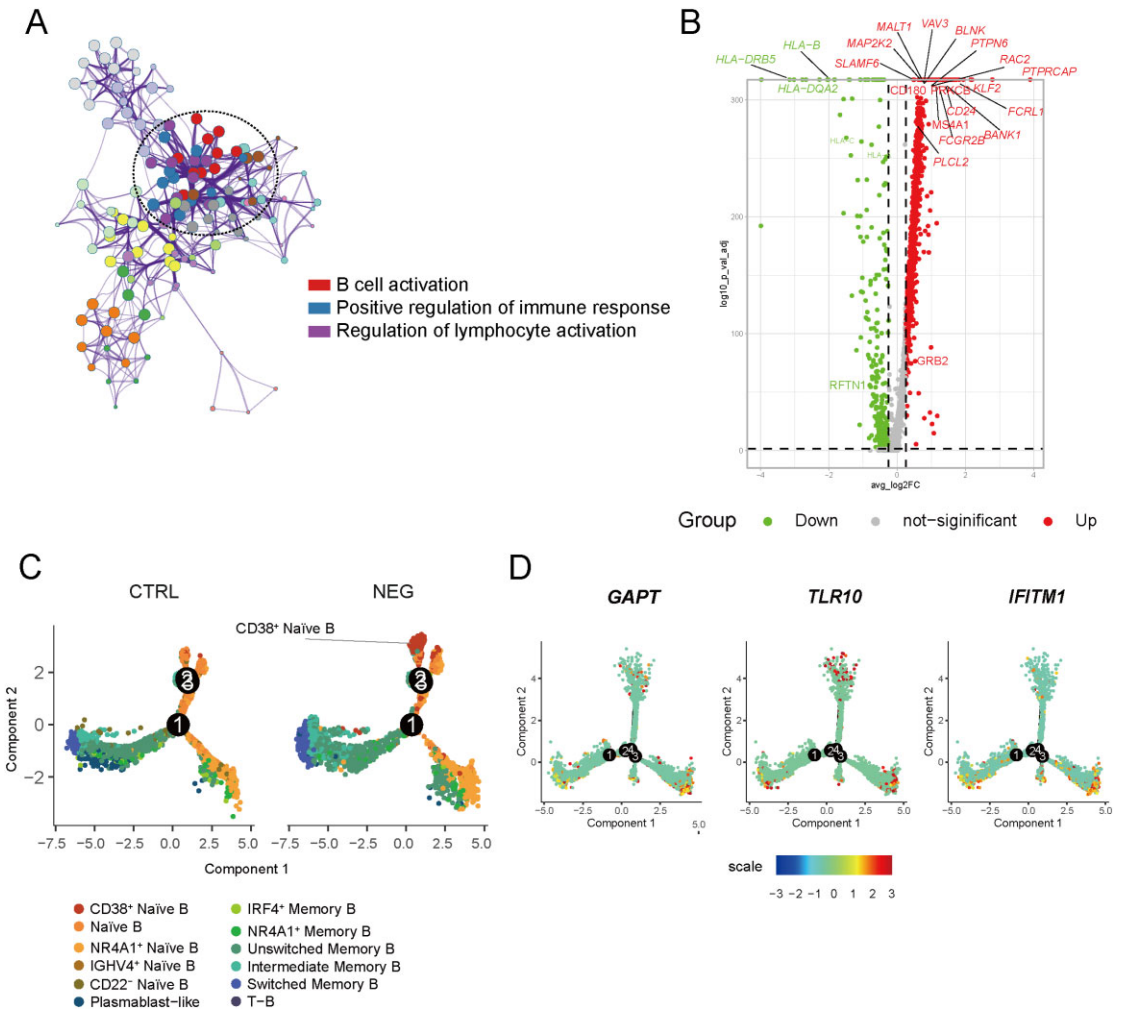

Figure 2: Molecular features of CD38⁺ naïve B cells in NEG. **(A)** GO analysis indicated the main related biological process of CD38⁺ naïve B cells. Genes involved in the analysis were DEGs between CD38⁺ naïve B cells and all other cell subsets ($P > .05$). **(B)** Volcano plots show DEGs in CD38⁺ naïve B cells of NEG compared with CTRL. Red dots represent significantly upregulated genes in NEG, green dots represent significantly downregulated genes in NEG and grey dots represent genes with no significant difference between NEG and CTRL. Particular genes are labelled with the gene name. **(C)** Pseudotime trajectory of all B cell subsets. **(D)** Pseudotime trajectory plots denote the expression of genes enriched in a particular branch, including *GAPT*, *TLR10* and *IFITM1*.

glucocorticoids, without immunosuppressant therapy, and still had massive proteinuria, which was in the acute stage of the disease. We obtained the scRNA-seq data of CD19⁺ cells from the peripheral blood of NEG. We integrated public data on peripheral blood samples from paediatric individuals ($n = 6$), which served as controls (CTRLs) (Fig. 1A, Supplementary Table S5) [17]. We performed reclustering analysis and obtained 13 clusters of B cells (Supplementary Figure S2A–C), which were then annotated into 12 cell subsets (Fig. 1B and C, Supplementary Table S6). The percentage of CD38⁺ naïve B cell subsets in NEG was higher than those in CTRL (Fig. 1C and D). The lymphocyte activation, B cell receptor and antigen processing and presentation–related pathway are enhanced in each B cell subset of NEG (Fig. 1E, Supplementary Figure S2D). In addition, the viral process pathway was also activated in NEG (Supplementary Figure S2D). The results of the gene set score also confirmed our findings (Supplementary Figure S2E). Some viral infections were closely associated with the development of MN, such as hepatitis B virus [18], syphilis [19] and coronavirus disease 2019 [20]. NEG had no clinical evidence of viral infection, but both circulating naïve B cells and memory B cells showed virus-related changes.

Activated CD38⁺ naïve B cells expanded in NEG

CD38⁺ naïve B cells (Supplementary Figure S3A) in NEG were not only increased in cell number, but also exhibited activated lymphocyte activation function (Fig. 1E). Previous studies have suggested that glucocorticoids (GCs) can induce a decrease in the number of this cell subset [21]. The results of GC-related gene set–based score analysis (Supplementary Figure S2F) and flow cytometry analysis (Supplementary Figure S2G) indicated that CD38⁺ naïve B cells were markedly increased in the disease condition but not induced by GCs. Functional enrichment analysis of signature genes found that the CD38⁺ naïve B cell subset was mainly related to B cell activation and positive regulation of the immune response (Fig. 2A). *VAV3*, *RAC2*, *BLNK*, *GRB2*, *MAP2K2* and *MALT1* were significantly upregulated in NEG and *HLA-A*, *HLA-B*, *HLA-C* and *HLA-DQA2* were significantly downregulated in NEG compared with those in the CTRL group (Fig. 2B). CD38⁺ naïve B cells were highly enriched at the start of pseudotime trajectory (Fig. 2C, Supplementary Figure S3B). *GAPT*, *TLR10* and *IFITM1* were significantly expressed in CD38⁺ naïve B cells, suggesting a potential important role in the differentiation process (Fig. 2D).

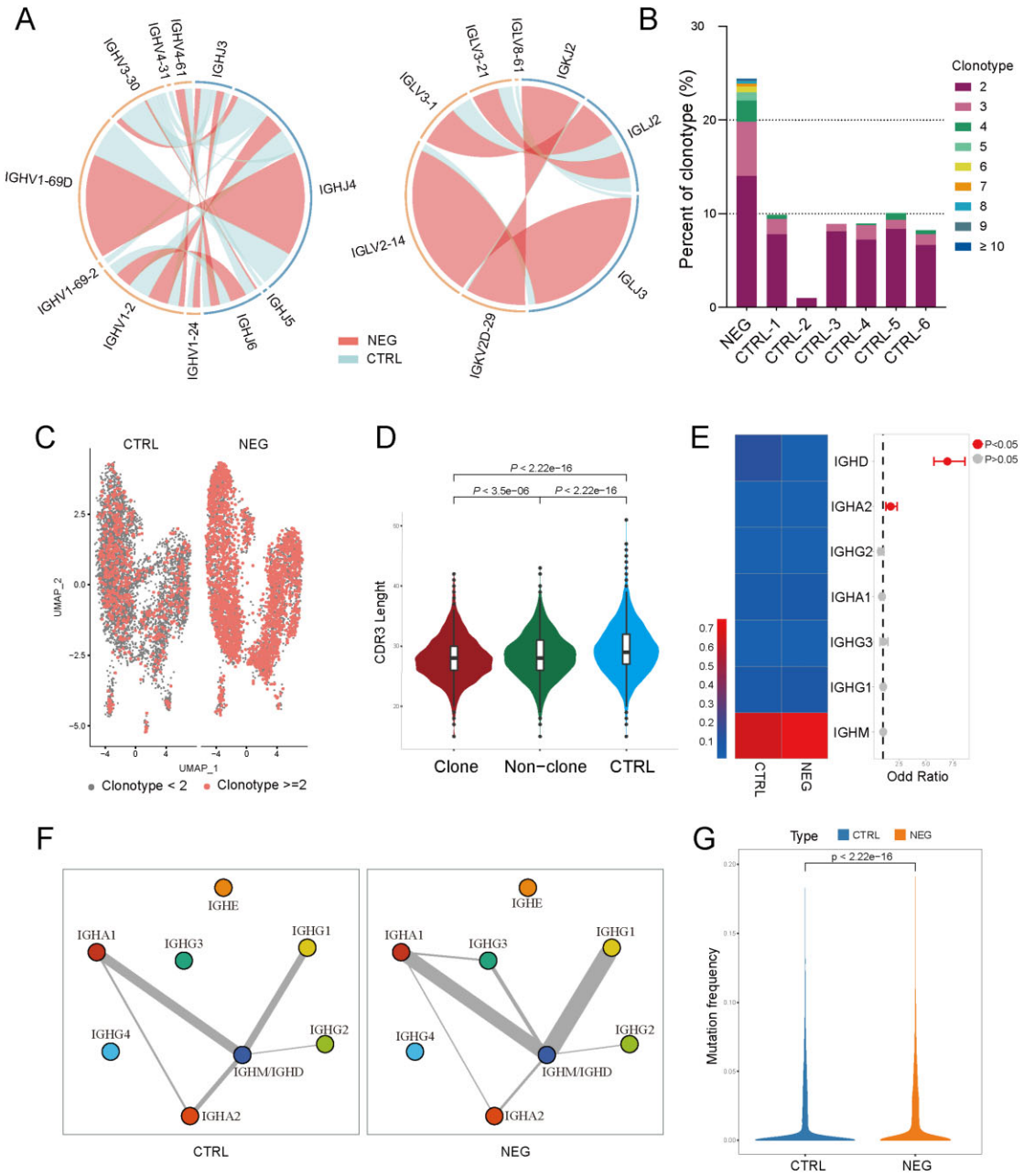

Figure 3: Features of BCR in NEG. **(A)** Circos plots show the differential heavy (left) and light (right) VJ pairs in NEG and CTRL. Red links represent NEG-specific VJ pairs and blue links represent CTRL-specific VJ pairs. **(B)** Bar plots show the relative percentage of each clonal expansion status by individual sample. The colour blocks represent different clonal expansion status. **(C)** UMAP plots show the distribution of clonally expanded B cells. **(D)** The distribution of CDR3 length in the clonal expanded and non-clonal expanded B cells of NEG and B cells of CTRL. **(E)** Heatmap plots show the difference in immunoglobulin isotypes between CTRL and NEG. The colours represent the P-value of the significant positive or negative; red: $P < .05$, grey: $P > .05$. **(F)** Class-switching events in CTRL and NEG. The thickness of the line indicates the number of sharing clonotypes between two immunoglobulin isotypes. **(G)** The differential analysis of somatic hypermutation rate between CTRL and NEG. Blue and orange represent CTRL and NEG, respectively.

Clonal expansion of both naïve and memory B cell subsets in NEG

The BCR lineage signature is an important part of the immune environment in MN [12]. For the VJ pair of the heavy chain, the frequency of IGHV3-30/IGHJ4 was significantly reduced in NEG (Fig. 3A). For the VJ pair of the light chain, the frequency of IGLV2-14/IGLJ3 and IGKV2D-29/IGKJ2 was significantly increased in NEG (Fig. 3A). The proportion of clonally expanded B cells (clone size >1) in NEG was 24.38%, while the proportion in CTRL was only 7.85% (Fig. 3B, Supplementary Figure S3C). Surprisingly, both naïve and memory B cell subsets in NEG showed clonal expansion (Fig. 3C, Supplementary Figure S3D). In addition, the CDR3 length of NEG clonally expanded B cells was significantly shorter than that of NEG non-clonally expanded B cells and CTRL cells (Fig. 3D). In NEG, the levels of IGHD and IGHA2 were significantly increased and the level of IGHM was also increased (no significant difference), suggesting their correlation with the

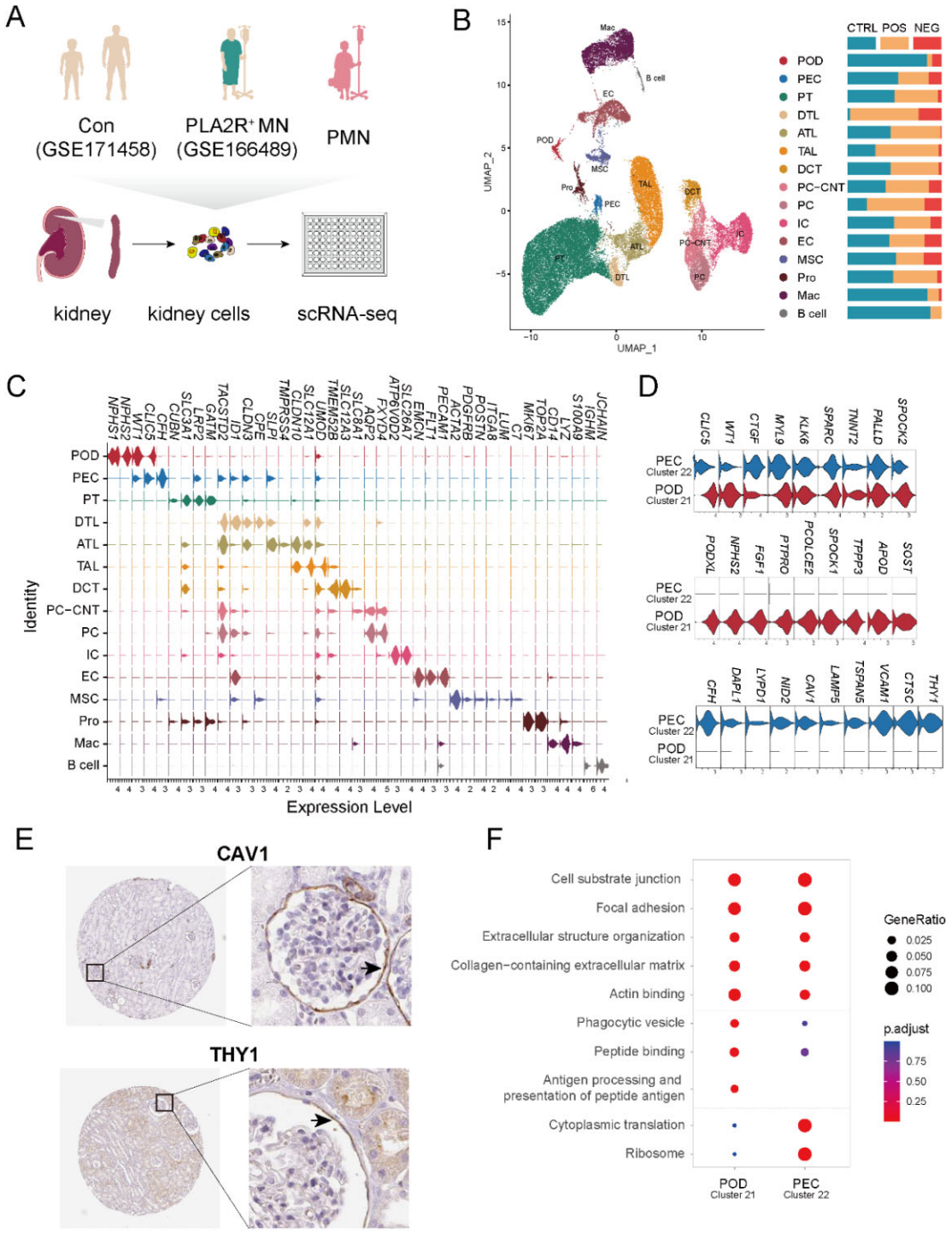

Figure 4: Similarities and differences of molecular features between podocytes and PECs. **(A)** The experimental workflow of scRNA-seq in kidney cells. **(B)** UMAP plots of cells from all merged samples, coloured by cell type. Each dot represents an individual cell. Bar plots show the proportion of CTRL, POS and NEG in each cell type. Blue, orange and red represent samples collected from CTRL, POS and NEG, respectively. **(C)** Violin plots of the selected marker genes in all kidney cell types. **(D)** Violin plots show the normalized expression level of marker genes in PECs and podocytes. The x-axis is log scale normalized read count. **(E)** Human Protein Atlas images show proteins encoded by new marker genes of PECs. Partial images enlargement ratio 1:4. Images are available from https://www.proteinatlas.org/. **(F)** GO biological process analysis of podocytes and PECs. The size of the dots represents the gene ratio and the redder colour key indicates the smaller adjusted *P*-value. POD: podocytes; DTL: descending thin limb; ATL: thin ascending limb; TAL: thick ascending limb; DCT: distal convoluted tubule; PC-CNT; principal cells-connecting tubule; PC: principal cells; IC: intercalated cells; EC: endothelial cells; MSC: mesenchymal stromal cells; Pro: proliferating cells; Mac: macrophage.

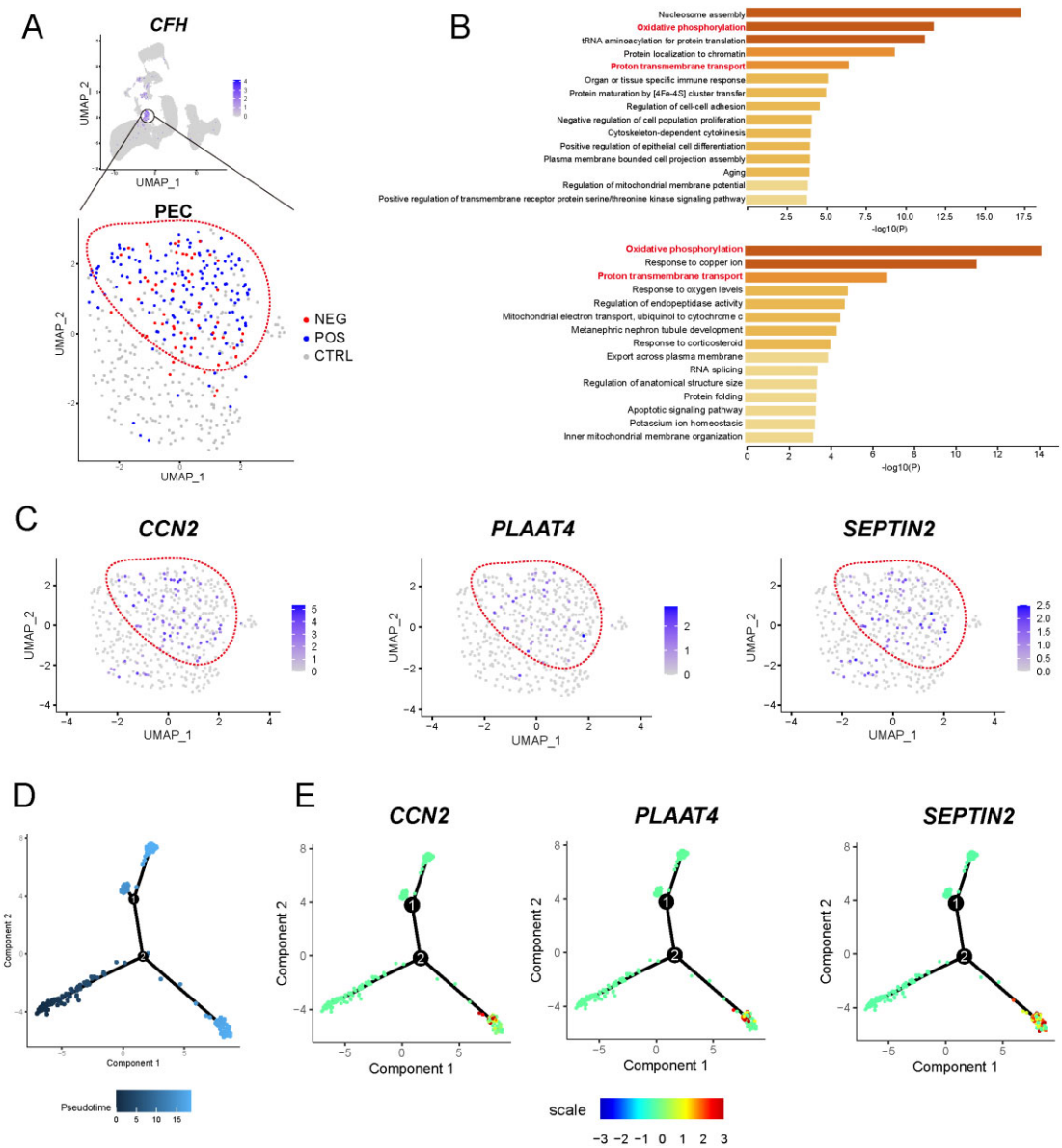

Figure 5: Molecular features of PECs in NEG. **(A)** UMAP plots show the marker gene *CFH* of PEC (UP) and the reclustered PEC (DOWN). Red, blue and grey represent cells from NEG, POS and CTRL, respectively. **(B)** GO biological process analysis of upregulated DEGs in PEC of NEG (UP) and POS (DOWN) compared with CTRL. GO terms are labelled with name and sorted by −log10 (*P*) value. A darker colour indicates a smaller *P*-value. The top 15 enriched GO terms are shown. Interesting terms are labelled in red. **(C)** UMAP plots show the expression of marker genes *CCN2*, *PLAAT4* and *SEPTIN2* in reclustered PECs. Red curve marks the location of cells derived from NEG and POS samples. **(D)** Pseudotime trajectory of the reclustered PEC subset. **(E)** Pseudotime trajectory plots denote the expression of genes enriched in a particular branch, including *CCN2*, *PLAAT4* and *SEPTIN2*.

disease (Fig. 3E). CSR plays an important role in the immune response to disease [22]. CSR analysis showed that the switching between immunoglobulin M (IgM)/D and IgG1 was increased in NEG. The switching between IgM/D and IgG3 occurred in NEG, as well as IGA1 and IgG3 (Fig. 3F). SHM was more frequent in NEG than in CTRL (Fig. 3G), suggesting maturation of antibody affinity.

Significant changes in PECs of NEG

We integrated the kidney scRNA-seq data of NEG ($n = 1$), POS ($n = 6$) and CTRL ($n = 4$) (Fig. 4A, Supplementary Table S5) [15]. We annotated 24 clusters as 15 cell subsets by marker genes (Fig. 4B and C, Supplementary Table S7). Podocytes are closely related to the pathogenic mechanism of MN [8]. The classic marker genes of podocytes had significant expression in both clusters 21 and 22, including *WT1*, *MYL9* and *CLIC5* (Fig. 4D). Cluster 22 significantly expressed *CFH* and *VCAM1* and was defined as PECs (Fig. 4D, Supplementary Figure S4A and B) [23]. In addition, we found new marker genes that differentiated PECs (cluster 22) from podocytes (cluster 21), including *NID2*, *CAV1* and *THY1* (Fig. 4D and E, Supplementary Figure S4A and B). The functions of phagocytic vesicles, peptide binding and antigen processing and presentation of peptide antigen were more evident in podocytes (Fig. 4F). PECs may play a replacement role after podocyte injury and shedding [24, 25]. PECs of the disease

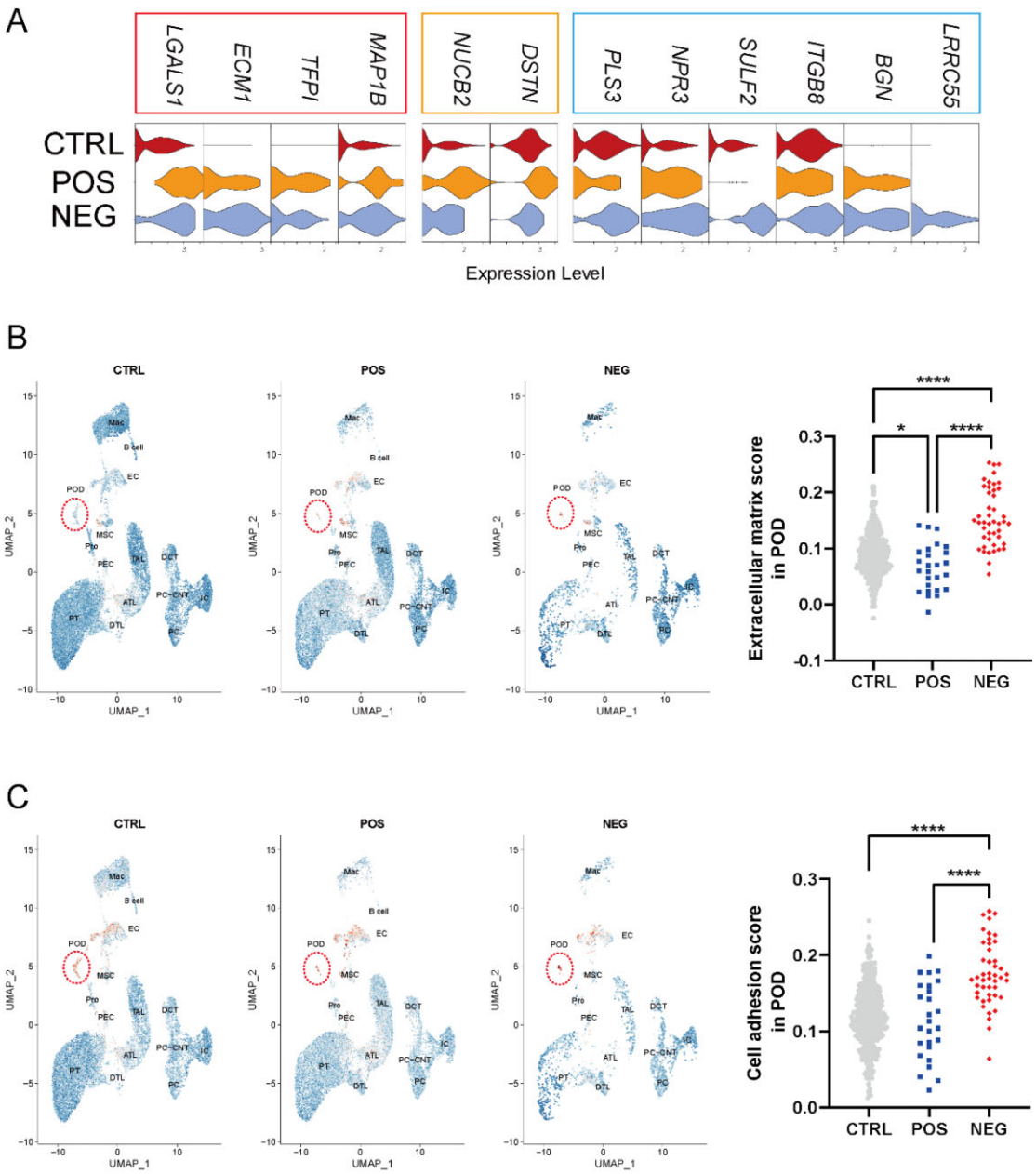

Figure 6: Molecular features of podocytes in NEG. **(A)** Violin plots show the particular gene expression of podocytes in each group. CTRL, POS and NEG are shown in different colours. Normalized expression levels are shown. **(B, C)** UMAP plots and scatter plots show the expression levels of particular GO terms across clusters derived from CTRL, POS and NEG. On the left, the colour key from blue to red indicates low to high expression level. On the right, groups are shown in different colours. GO terms are about extracellular matrix **(B)** and cell adhesion **(C)** with details in Supplementary Table S4. All differences with $P < .05$ are indicated. *$P < .05$, ****$P < .0001$. POD: podocytes.

group (NEG and POS) and CTRLs showed obvious differences (Fig. 5A), suggesting that PECs might have undergone significant changes in the disease. The functional enrichment results of DEGs in PECs suggested that oxidative phosphorylation and proton transmembrane transport were upregulated in NEG and POS (Fig. 5B, Supplementary Figure S5A). In PECs of NEG, cellular communication network factor-related genes (*CCN1*, *CCN2* and *CCN6*), phospholipase A and acyltransferase family genes (*PLAAT4* and *PLAAT3*) and septin family genes (*SEPTIN2* and *SEPTIN7*) were significantly upregulated (Fig. 5C, Supplementary Figure S5B). Pseudotime trajectory analysis showed that PECs in NEG and POS distributed in different trajectory branches (Fig. 5D, Supplementary Figure S5C). On the trajectory branch of NEG, *CCN2*, *PLAAT4*, *SEPTIN2* and other genes were significantly expressed (Fig. 5E), which might represent the molecular characteristics of PECs in NEG.

Activated cell adhesion and extracellular matrix functions of podocytes in NEG

Podocyte injury in MN leads directly to proteinuria and involves distal nephrons [1]. *LGALS1*, *ECM1*, *TFPI* and *MAP1B* were all

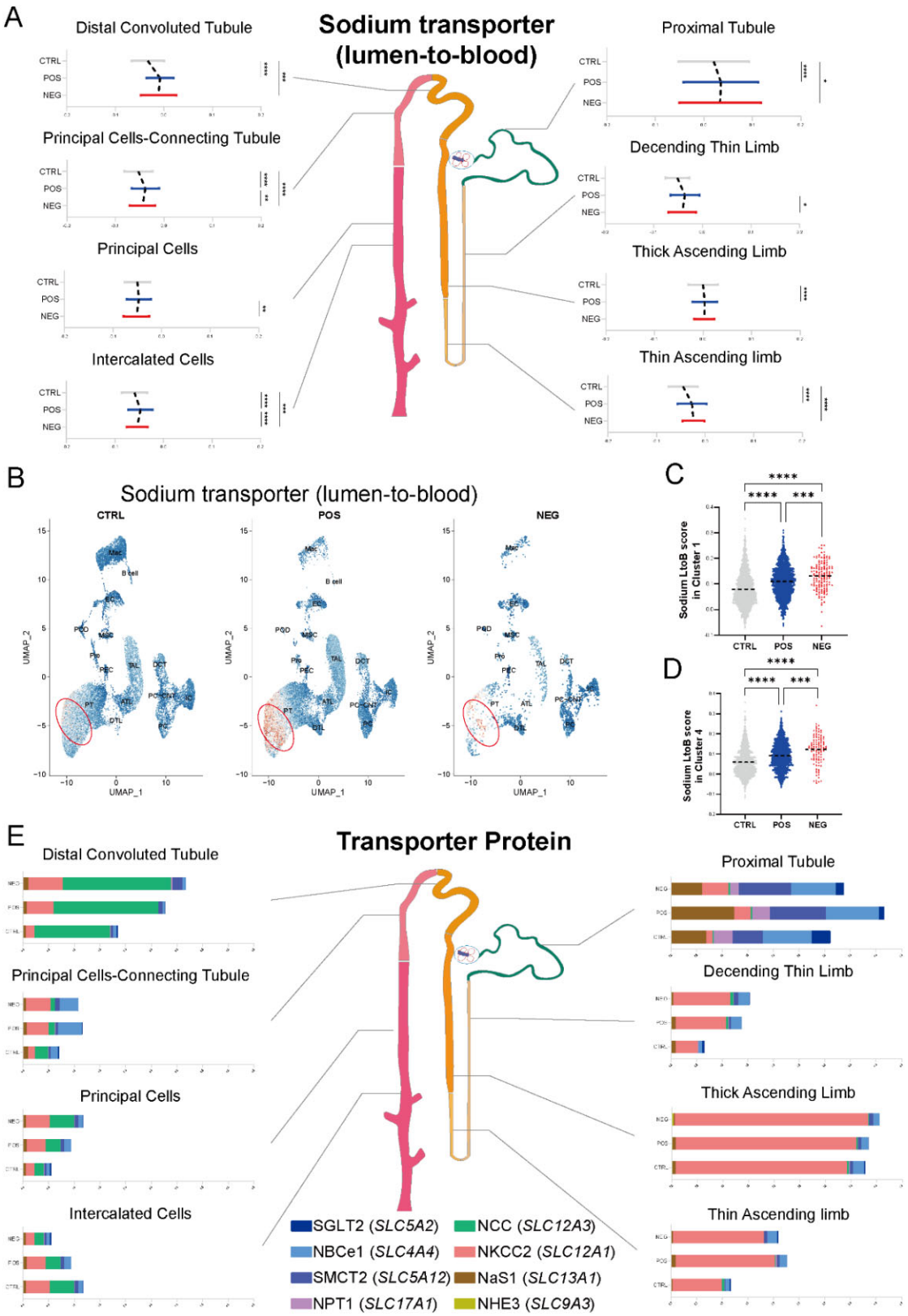

Figure 7: Sodium transport capacity in each segment of renal tubule in MN. **(A)** Comparison of LtoB gene set–based scores of each renal tubule segment among CTRL, POS and NEG. All differences with $P < .05$ are indicated. *$P < .05$, **$P < .01$, ***$P < .001$ and ****$P < .0001$. **(B)** UMAP plots show LtoB gene set–based scores across clusters derived from CTRL, POS and NEG. The colour key from blue to red indicates low to high expression level. **(C, D)** Scatter plots show LtoB gene set–based scores in cluster 1 **(C)** and cluster 4 **(D)**. Groups are shown in different colours. Horizontal lines represent median values. All differences with $P < .05$ are indicated. ***$P < .001$, ****$P < .0001$. **(E)** The expression levels were compared including particular genes involved in sodium lumen-to-blood transport for each segment of the renal tubule in CTRL, POS and NEG. The proteins encoded by particular genes are marked below.

significantly upregulated in podocytes of the disease group. *NUCB2* and *DSTN* were significantly upregulated in the podocytes of POS, while *NPR3*, *SULF2*, *ITGB8*, *BGN* and *LRRC55* were significantly upregulated in podocytes of NEG (Fig. 6A). Significantly upregulated genes in the podocytes of NEG were associated with functions such as positive regulation of cell migration and cell adhesion (Supplementary Figure S6A). Subepithelial immune deposits were closely related to the processes of extracellular matrix and cell adhesion [26]. The gene set score comparison confirmed that the extracellular matrix and cell adhesion gene sets in the podocytes of NEG were significantly increased (Fig. 6B and C, Supplementary Figure S6B and C). *LRRC55* was significantly upregulated in NEG, and previous studies have suggested that altered calcium channels associated with *LRRC55* may be one of the key mechanisms of podocyte injury [27]. The calcium channel gene set score was indeed significantly increased in podocytes of NEG (Supplementary Figure S6D).

Changes in sodium transport in each segment of the renal tubule in pMN

Oedema is the main clinical manifestation in NS patients, including those with MN, which may be related to sodium retention in distal nephrons [28]. We defined genes involved in sodium lumen-to-blood transport as LtoB [29]. Gene set–based scores for LtoB in each cell subset were calculated (Supplementary Table S4). In the proximal tubule (PT), thin ascending limb and distal convoluted tubule, both POS and NEG had significantly increased LtoB gene set–based scores compared with CTRLs, but there was no significant difference between POS and NEG (Fig. 7A). According to the UMAPs (Fig. 7B), we focused on clusters 1 and 4 in the PT. In these two clusters, scores of the LtoB gene set were significantly increased in both POS and NEG compared with CTRLs, and the score was significantly higher in NEG than in POS (Fig. 7C and D). SMCT2, encoded by *SLC5A12*, and Na-bicarbonate cotransporter e1 (NBCe1), encoded by *SLC4A4*, were the major sodium transporters (Fig. 7E). Surprisingly, the expression of *SLC5A12* in NEG was significantly increased in clusters 1 and 4 of the PT (Supplementary Figure S6E).

DISCUSSION

Due to the low incidence of MN in children and the low rate of renal biopsy, there are few studies on MN in children [30]. The child included in this study had typical clinical manifestations and pathological changes of MN and common secondary factors were excluded (Supplementary Table S1). Even more rarely, the kidney of the child was negative for seven classical podocyte autoantibodies. At present, there are few studies on anti-PLA2R antibody-negative pNMs, and there is even a lack of comparative studies on pNMs with different autoantibodies. Our results are the first to demonstrate transcriptome changes in kidney cell subsets of POS and NEG patients. There were significant differences between the disease group and CTRLs in each kidney cell type, but no significant difference was found between NEG and POS. The results suggest that different types of MN classified by autoantibodies had similar changes in kidney molecular features.

MN is now considered an autoimmune disease confined to the kidney [31]. Our study found that both naïve B cells and memory B cells in NEG had undergone significant changes, including cell number, characteristic gene, molecular function and clonal type. This result indicated that both naïve B cells and memory B cells play an important role in the production of autoantibodies. Breg cells can reduce inflammatory responses through the action of immune regulatory cytokines and other mechanisms and help maintain immune tolerance [32]. In our study, the expanded and activated $CD38^+$ naïve B cells in NEG had the molecular characteristics of Breg cells ($CD19^+CD24^+CD27^-CD38^+$) (Supplementary Figure S3A). Breg cells with such molecular characteristics exerted immunosuppressive effects by secreting cytokines, such as interleukin-10 [32, 33]. Our study indicated that $CD38^+$ naïve B cells may play a key role in the circulating immune environment in pMN. More clinical and functional studies are needed to clarify the function and significance of this cell subset.

Increased volume overload is a classic pathophysiological feature of NS represented by MN. Controlling and improving volume overload is the key clinical method for improving the long-term prognosis and complications of NS [28]. Our study found that in NEG and POS patients, both distal nephrons, such as LOH, and a group of PT cells showed significant increases in the expression of sodium transporters (Fig. 7A). Among these transporter genes, the expression level of *SLC5A12*, encoding SMCT2, was significantly increased (Fig. 7E). It is necessary to consider the effect of the changes in expression level of SMCT2 in PT on sodium transport in NS, as this may be one of the mechanisms involved in water and sodium retention.

This high-throughput multi-omics research on a rare case of a NEG patient who was limited and observational, which needs clinical cohort validation and systematic mechanistic research with larger sample sizes [34, 35]. As with scRNA-seq studies of other glomerular diseases [36], the number of glomerular cells captured in this study was limited. With the continuous development of omics technologies, such as spatial transcriptomics and spatial proteomics [37], the current understanding of glomerular diseases will be greatly improved.

SUPPLEMENTARY DATA

Supplementary data are available at *ckj* online.

ACKNOWLEDGEMENTS

We sincerely thank all participants in this study.

FUNDING

This work was supported by the National Key R&D Program of China (2022YFC2705101), Program for Youth Innovation in Future Medicine, Chongqing Medical University (W0098) and Natural Science Foundation of Chongqing (cstc2021jcyj-bsh0053).

AUTHORS' CONTRIBUTIONS

H.Y. and Q.L. conceived the study. X.F. analysed the data and wrote the manuscript with assistance from Q.C., J.Z., S.Y., Y.W., Y.J., J.W., L.L., H.J., L.P. and A.W. G.Z. and M.W. reviewed the manuscript. All authors contributed to the article and approved the submitted version.

DATA AVAILABILITY STATEMENT

All raw and processed data are available from the corresponding author upon reasonable request.

CONFLICT OF INTEREST STATEMENT

Y.W. and L.L. are employed by the Nanjing Jiangbei New Area Biopharmaceutical Public Service Platform. The remaining authors declare that the research was conducted in the absence of any commercial or financial relationships that could be construed as a potential conflict of interest. Parts of the study have been accepted as a Moderated Oral at the 60th ERA Congress and was awarded "Best Abstracts presented by young".

REFERENCES

1. Ronco P, Beck L, Debiec H *et al*. Membranous nephropathy. *Nat Rev Dis Primers* 2021;**7**:69. https://doi.org/10.1038/s41572-021-00303-z
2. Sethi S. New 'antigens' in membranous nephropathy. *J Am Soc Nephrol* 2021;**32**:268–78. https://doi.org/10.1681/ASN.2020071082
3. Beck LH, Jr, Bonegio RG, Lambeau G *et al*. M-type phospholipase A2 receptor as target antigen in idiopathic membranous nephropathy. *N Engl J Med* 2009;**361**:11–21. https://doi.org/10.1056/NEJMoa0810457
4. Van De Logt AE, Fresquet M, Wetzels JF *et al*. The anti-PLA2R antibody in membranous nephropathy: what we know and what remains a decade after its discovery. *Kidney Int* 2019;**96**:1292–302. https://doi.org/10.1016/j.kint.2019.07.014
5. Tomas NM, Beck LH, Jr, Meyer-Schwesinger C *et al*. Thrombospondin type-1 domain-containing 7A in idiopathic membranous nephropathy. *N Engl J Med* 2014;**371**:2277–87. https://doi.org/10.1056/NEJMoa1409354
6. Caza TN, Hassen SI, Dvanajscak Z *et al*. NELL1 is a target antigen in malignancy-associated membranous nephropathy. *Kidney Int* 2021;**99**:967–76. https://doi.org/10.1016/j.kint.2020.07.039
7. Sethi S, Debiec H, Madden B *et al*. Semaphorin 3B-associated membranous nephropathy is a distinct type of disease predominantly present in pediatric patients. *Kidney Int* 2020;**98**:1253–64. https://doi.org/10.1016/j.kint.2020.05.030
8. Hoxha E, Reinhard L, Stahl, RAK. Membranous nephropathy: new pathogenic mechanisms and their clinical implications. *Nat Rev Nephrol* 2022;**18**:466–78. https://doi.org/10.1038/s41581-022-00564-1
9. So BYF, Yap DYH, Chan TM. B cells in primary membranous nephropathy: escape from immune tolerance and implications for patient management. *Int J Mol Sci* 2021;**22**:13560. https://doi.org/10.3390/ijms222413560
10. Rosenzwajg M, Languille E, Debiec H *et al*. B- and T-cell subpopulations in patients with severe idiopathic membranous nephropathy may predict an early response to rituximab. *Kidney Int* 2017;**92**:227–37. https://doi.org/10.1016/j.kint.2017.01.012
11. Cantarelli C, Jarque M, Angeletti A *et al*. A comprehensive phenotypic and functional immune analysis unravels circulating anti-phospholipase A2 receptor antibody secreting cells in membranous nephropathy patients. *Kidney Int Rep* 2020;**5**:1764–76. https://doi.org/10.1016/j.ekir.2020.07.028
12. Su Z, Jin Y, Zhang Y *et al*. The diagnostic and prognostic potential of the B-cell repertoire in membranous nephropathy. *Front Immunol* 2021;**12**:635326. https://doi.org/10.3389/fimmu.2021.635326
13. Sealfon R, Mariani L, Avila-Casado C *et al*. Molecular characterization of membranous nephropathy. *J Am Soc Nephrol* 2022;**33**:1208–21. https://doi.org/10.1681/ASN.2021060784
14. Cremoni M, Brglez V, Perez S *et al*. Th17-Immune response in patients with membranous nephropathy is associated with thrombosis and relapses. *Front Immunol* 2020;**11**:574997. https://doi.org/10.3389/fimmu.2020.574997
15. Xu J, Shen C, Lin W *et al*. Single-cell profiling reveals transcriptional signatures and cell-cell crosstalk in Anti-PLA2R positive idiopathic membranous nephropathy patients. *Front Immunol* 2021;**12**:683330. https://doi.org/10.3389/fimmu.2021.683330
16. Tang R, Meng T, Lin W *et al*. A partial picture of the single-cell transcriptomics of human IgA nephropathy. *Front Immunol* 2021;**12**:645988. https://doi.org/10.3389/fimmu.2021.645988
17. Ramaswamy A, Brodsky NN, Sumida TS *et al*. Immune dysregulation and autoreactivity correlate with disease severity in SARS-CoV-2-associated multisystem inflammatory syndrome in children. *Immunity* 2021;**54**:1083–1095.e7. https://doi.org/10.1016/j.immuni.2021.04.003
18. Yu L, Lin W, Shen C *et al*. Intrarenal single-cell sequencing of hepatitis b virus associated membranous nephropathy. *Front Med* 2022;**9**:869284. https://doi.org/10.3389/fmed.2022.869284
19. Sethi S, Madden B, Casal Moura M *et al*. Membranous nephropathy in syphilis is associated with neuron-derived neurotrophic factor. *J Am Soc Nephrol* 2023;**34**:374–84. https://doi.org/10.1681/ASN.0000000000000061
20. Ma Q, Li X, Xu G. New-onset and relapsed membranous nephropathy post SARS-CoV-2 and COVID-19 vaccination. *Viruses* 2022;**14**:2143. https://doi.org/10.3390/v14102143
21. Rebollo-Mesa I, Nova-Lamperti E, Mobillo, P *et al*. Biomarkers of tolerance in kidney transplantation: are we predicting tolerance or response to immunosuppressive treatment? *Am J Transplant* 2016;**16**:3443–57. https://doi.org/10.1111/ajt.13932
22. Cyster JG, Allen CDC. B cell responses: cell interaction dynamics and decisions. *Cell* 2019;**177**:524–40. https://doi.org/10.1016/j.cell.2019.03.016
23. Bronstein R, Pace J, Gowthaman Y *et al*. Podocyte-parietal epithelial cell interdependence in glomerular development and disease. *J Am Soc Nephrol* 2023;**34**:737–50. https://doi.org/10.1681/ASN.0000000000000104
24. Shankland SJ, Smeets B, Pippin JW *et al*. The emergence of the glomerular parietal epithelial cell. *Nat Rev Nephrol* 2014;**10**:158–73. https://doi.org/10.1038/nrneph.2014.1
25. Melica ME, Antonelli G, Semeraro R *et al*. Differentiation of crescent-forming kidney progenitor cells into podocytes attenuates severe glomerulonephritis in mice. *Sci Transl Med* 2022;**14**:eabg3277. https://doi.org/10.1126/scitranslmed.abg3277
26. Benzing T, Salant D. Insights into glomerular filtration and albuminuria. *N Engl J Med* 2021;**384**:1437–46. https://doi.org/10.1056/NEJMra1808786.
27. Hu S, Han R, Chen L *et al*. Upregulated LRRC55 promotes BK channel activation and aggravates cell injury in podocytes. *J Exp Med* 2021;**218**:e20192373. https://doi.org/10.1084/jem.20192373
28. Siddall EC, Radhakrishnan J. The pathophysiology of edema formation in the nephrotic syndrome. *Kidney Int* 2012;**82**:635–42. https://doi.org/10.1038/ki.2012.180
29. Hansen J, Sealfon R, Menon R *et al*. A reference tissue atlas for the human kidney. *Sci Adv* 2022;**8**:eabn4965. https://doi.org/10.1126/sciadv.abn4965
30. Safar-Boueri L, Piya A, Beck LH, Jr *et al*. Membranous nephropathy: diagnosis, treatment, and monitoring in the post-PLA2R era. *Pediatr Nephrol* 2021;**36**:19–30. https://doi.org/10.1007/s00467-019-04425-1

31. Kidney Disease: Improving Global Outcomes Glomerular Diseases Work Group. KDIGO 2021 clinical practice guideline for the management of glomerular diseases. *Kidney Int* 2021;**100**(4 Suppl):S1–S276. https://doi.org/10.1016/j.kint.2021.05.021
32. Oleinika K, Mauri C, Salama AD. Effector and regulatory B cells in immune-mediated kidney disease. *Nat Rev Nephrol* 2019;**15**:11–26. https://doi.org/10.1038/s41581-018-0074-7
33. Dong Z, Liu Z, Dai H *et al*. The potential role of regulatory B cells in idiopathic membranous nephropathy. *J Immunol Res* 2020;**2020**:7638365. https://doi.org/10.1155/2020/7638365.
34. Perez RK, Gordon MG, Subramaniam M *et al*. Single-cell RNA-seq reveals cell type-specific molecular and genetic associations to lupus. *Science* 2022;**376**:eabf1970. https://doi.org/10.1126/science.abf1970
35. Yazar S, Alquicira-Hernandez J, Wing K *et al*. Single-cell eQTL mapping identifies cell type-specific genetic control of autoimmune disease. *Science* 2022;**376**:eabf3041. https://doi.org/10.1126/science.abf3041
36. Deleersnijder D, Callemeyn J, Arijs I *et al*. Current methodological challenges of single-cell and single-nucleus RNA-sequencing in glomerular diseases. *J Am Soc Nephrol* 2021;**32**:1838–52. https://doi.org/10.1681/ASN.2021020157
37. Rao A, Barkley D, Franca GS *et al*. Exploring tissue architecture using spatial transcriptomics. *Nature* 2021;**596**:211–20. https://doi.org/10.1038/s41586-021-03634-9

Received: 12.5.2023; Editorial decision: 2.8.2023